Medical Image Segmentation and Applications

Lab 1: Image Pre-processing

Submitted By

Md. Kamrul Hasan

Fakrul Islam Tushar

Submitted To

Robert Martí Marly, PhD

robert.marti@udg.edu

October 28, 2018

Contents of the report **Page No**

1. Introduction

Almost in every image processing or analysis work, image pre-preprocessing is crucial step. In medical image analysis, pre-processing is a very important step because the further success or performance of the algorithm mostly dependent on pre-processed image. In this lab, we are working with 3D Brain MRI data. In case of working with brain MRI removing the noise and bias field (which is due to inhomogeneity of the magnetic field) is very important part of pre-processing of brain MRI. To do so, we widely used algorithm Anisotropic diffusion, isotropic diffusion which can diffuse in any direction, and Multiplicative intrinsic component optimization (MICO) have been used for noise removal and bias field correction respectfully. Both quantitative and qualitative performance of the algorithms also have been analyzed.

2. Method

The methods used for this lab are described briefly in the following sub-section.

2.1 Anisotropic diffusion

Avoid the undesirable effect of linear filtering such as blurring the meaningful edges of the image, Anisotropic Diffusion (AD) a non-linear partial differential equation-based diffusion process proposed by Perona and Malik become an obvious choice for image smoothing, edge detection, image segmentation and image enhancement [1]. AD method can successfully smooth noise, while respecting the region boundaries and small structures within the image, if some of its crucial parameters are estimated correctly. The basic AD equation presented by Perona and Malik in [1] can be expressed mathematically by the following equation.

$$\frac{\partial(x,y,t)}{\partial t} = div(g||\nabla I(x,y,t)||\nabla I(x,y,t))$$

Where, $t = Time\ Parameter$, $I(x,y,0) = Original\ Image$, $g = Conductance\ function$ $I(x,y,t) = gradient\ of\ the\ version\ of\ the\ image\ at\ time\ t$,

This conductance function is used to choose diffusion criteria. If this g(x)=1, the diffusion is maximal within the uniform region, and if g(x)=0, diffusion stopped across edges. Perona and Malik proposed 2 conductance function. conductance function $g_1 and\ g_2$. the conductance function g_1 favours high-contrast edges over low-contrast ones, while the g_2 function favors wide regions over smaller ones [1].

$$g_1 = e^{[-(\frac{x}{k})^2]} \text{ and } g_2 = \frac{1}{1+(\frac{x}{k})^2}$$

Where, $k = Threshold\ parameter$ (*a soft threshold between the image gradients that are attributed to noise and those attributed to edges.*). Perona and Malik discretized their anisotropic diffusion equation to

$$I_{t+1} = I_t(s) + \frac{\lambda}{|\eta_s|}\sum_{p\epsilon\eta_s} g_k(|\nabla I_{s,p}|)\nabla I_{s,p}$$

Where, $I = Discretely\ sampled\ image$, $s = Pixel\ position\ in\ the\ discrete\ 2D\ grid$, $t = Iteration\ step$, $g = conductance\ function$, $\lambda = constand, \lambda\epsilon(0,1]\ determines\ the\ rate\ of\ diffussion$, $\eta_s = represents\ the\ spatial\ 4-pixel\ neighborhood\ of\ pixel\ at\ s$, $\nabla I_{s,p} = I_s(p) - I_t(s), p\epsilon\eta_s = \{N,S,E,W\}$ = Difference between neighboring pixels in each direction. By this implementation exact discretization of the continuous equation is not achieved as mentioned in [1]. However, it is favored due to its low computational complexity, preserving most of the properties of the continuous form [1].

2.2 Isotropic diffusion

Isotropic diffusion is the minor modification of the Anisotropic diffusion equation that can be achieved by changing the $g||\nabla I(x,y,t)||$ in Anisotropic diffusion. Mathematically,

$$\frac{\partial(x,y,t)}{\partial t} = div(g||\nabla I(x,y,t)||\nabla I(x,y,t))$$

If $g||\nabla I(x,y,t)||$= constant, then this equation represents an isotropic diffusion.

2.3 Multiplicative intrinsic component optimization (MICO)

Bias field correction also called intensity inhomogeneity which is due to the inhomogeneity of the magnetic field that depends on the strength of the magnetic field. Multiplicative intrinsic component optimization (MICO) is a state-of-art method for bias field correction and segmentation proposed by Li et al. at [2]. MICO is an energy minimization method and formulation of energy is convex in each of its variable, which provide robustness of the energy minimization algorithm. MICO algorithm decompose MRI images into two multiplicative intrinsic components [2].

$$I(x) = b(x)J(x) + n(x)$$

Where, $I(x) = Intensity\ of\ the\ observed\ Image\ at\ voxel\ x$, $J(x) = True\ Image$, $b(x) = Bias\ fiels$, $n(x) = Additive\ noise\ with\ zero\ mean$. The estimation of the bias field is given by

$$b(x) = w^T G(x)$$

Where, w= Column vector which represents the coefficients $w_{1,} \dots \dots \dots w_M$ by a column vector, G(x)= Column vector which represents the basis functions $g_1(x) \dots \dots \dots g_M(x)$. In [2] true image is approximated using the equation below,

$$J(x) = \sum_{i=1}^{N} c_i u_i$$

Where, $N = Number\ of\ voxel$, $c_i = constant\ for\ all\ the\ points\ x\ in\ the\ i\ th\ tissue$, $u_i = Fuzzy\ membership\ function\ for\ the\ point\ x\ in\ the\ i\ th\ tissue$. Li at al at [2] using this approximation of true image and bias field proposed the energy function shown below which is optimized in each iteration and update the values membership function u, bias field b and constant c.

$$F(u, c, w) = \int_{\Omega} |\, I(x) - w^T G(x) \sum_{i=1}^{N} c_i u_i \,|^2 dx$$

To achieve the fuzzy segmentation, the energy function F is further modified by introducing a fuzzifier q ≥ 1 [2].

$$F_q(u, c, w) = \int_{\Omega} |\, I(x) - w^T G(x) \sum_{i=1}^{N} c_i \,|^2 u_i^q(x) dx$$

For the case q >1, the optimal membership functions that minimize the energy F_q(u, c, w) are fuzzy membership functions, which take value between 0 and 1. this energy F_q(u, c, w) is that it is convex in each variable, u, c, or w. This property ensures that the energy F_q(u, c, w) has a unique minimum point in each of its variables [2].

3. Performance matric

3.1 Entropy difference

Entropy is a statistical measure of randomness that can be used to characterize the texture of the input image which can be defined mathematically by the following equation.

$Entropy = p \log_2(p)$, Where, p= Normalized histogram of the image.

In this lab, entropy difference between original image and processed image has been calculated by the follow equation.

$$Entropy\ differnce\ = Entropy_{original} - Entropy_{processed}$$

If $Entropy\ differnce = 0$, meaning that there is no difference of entropy between those two images. But, if $Entropy\ differnce = -ve$, meaning that entropy is increasing after processing and the more the negativity the more the increase of entropy after processing and vice-versa.

3.2 Tenengrad difference (TGD)

This measure is based on gradient measure maximization which is the value of an image J and calculated from the gradient ΔJ(x,y) where the partial derivatives are calculated using a sobel filter having convolution kernels along x and y axis [3]. Mathematically, TGD can be written as follows.

$$TGD = \sum_i \sum_j T(i,j)^2, \text{ Where, } T(i,j) = \sqrt{(J_X \otimes I(x,y))^2 + (J_y \otimes I(x,y))^2}$$

The quality of an image is high if its Tenengrad value is high which means that structural information of the image is high. In this lab, Tenengrad difference between original image and processed image has been calculated by the follow equation.

$$\text{TGD } differnce = TGD_{original} - TGD_{processed}$$

If $TGD\ differnce = 0$, meaning that there is no difference of Tenengrad between those two images. But, if $TGD\ differnce = -ve$, meaning that Tenengrad is increasing after processing and the more the negativity the more the increase of Tenengrad after processing and vice-versa.

3.3 Mean Square Error (MSE)

In statistics, the mean squared error (MSE) of an estimator measures the average of the squares of the errors and mathematically written as follows.

$$A = \frac{\sum_i \sum_j |X(i,j) - Y(i,j)|^2}{N}$$

Where, $X(i,j) = Input\ Image,\ Y(i,j) = output\ Image,\ N = Number\ of\ pixels$

3.4 Peak Signal to Noise Ratio (PSNR)

Peak signal-to-noise ratio, often abbreviated PSNR which is used to compute the amount of noise and that based on MSE. Mathematically, PSNR can be defined as follows [4].

$$PSNR = 10 \log_{10}(L-1)^2/MSE$$

Where, $L = Peak\ intensity\ level\ of\ the\ image$

3.5 Absolute Mean Brightness Error (AMBE)

To investigate whether the proposed method successfully maintains the input mean brightness, the absolute mean brightness error (AMBE) has been used [3].

$$AMBE = X_m - Y_m$$

where, $X_m = Mean\ of\ inpur\ image$ and $Y_m = Mean\ of\ output\ image$

3.6 Contrast Improvement Index (CII)

It measures the ratio of local contrast of comparing images. If the value of CII increases, then it shows improvement in contrast of an image [3].

$$CII = \frac{Y_{proposed}}{X_{original}}$$

where, $X_{original} = Average\ of\ the\ local\ contrast\ measured\ of\ input\ image$ and $Y_{proposed} = Average\ of\ the\ local\ contrast\ measured\ of\ output\ image.$

3.7 Structural Similarity Index (SSIM)

The Structural Similarity (SSIM) Index quality assessment index is based on the computation of three terms, namely the luminance term, the contrast term and the structural term [5].

$$SSIM = \frac{(2\mu_x\mu_y + C_1)(2\sigma_{xy} + C_2)}{(\mu_x + \mu_y + C_1)(\sigma_x + \sigma_y + C_2)}$$

Where,$\mu_x = Mean\ of\ Input\ image,\ \mu_y = Mean\ of\ Output\ image,\ \sigma_x = Standard\ deviation\ of\ Input\ image,\ \sigma_y = Standard\ deviation\ of\ Output\ image,\ \sigma_{xy} = Cross\ covarience\ of\ image$

3.8 Normalized Cross-correlation (NCC)

Normalized Cross-correlation (NCC) computes pixel-wise cross-correlation and normalized by the square root of the autocorrelation of the images which is invariant to linear differences between intensity distributions. Mathematically, NCC can be expressed as below-

$$NCC\left(I_{input}, I_{output}\right) = \frac{\sum_{x=0}^{X}\sum_{y=0}^{Y}\left(I_{input}(x,y) - \overline{I_{input}}\right) \times \left(I_{output}(x,y) - \overline{I_{output}}\right)}{\sqrt{\sum_{x=0}^{X}\sum_{y=0}^{Y}\left(I_{input}(x,y) - \overline{I_{output}}\right)^2 \times \sum_{x=0}^{X}\sum_{y=0}^{Y}\left(I_{output}(x,y) - \overline{I_{output}}\right)^2}}$$

4. Results and Discussions

For this lab work, there are five images in the data directory. The brief description about the objectives along with the data that have to do for this lab is shown in Table 1.

Table 1: Data set description along with processes require

S.L. No.	Data	Processed required
01	t1_icbm_normal_1mm_pn0_rf0.nii	Ground truth. So, no process requires.
02	t1_icbm_normal_1mm_pn0_rf20.nii	Bias field correction requires
03	t1_icbm_normal_1mm_pn0_rf40.nii	Bias field correction requires
04	t1_icbm_normal_1mm_pn1_rf0.nii	Denoising requires
05	t1_icbm_normal_1mm_pn5_rf0.nii	Denoising requires
06	t1_icbm_normal_1mm_pn5_rf20.nii	Both Bias field correction and denoising require

For the Bias field correction or denoising, following block diagram was used.

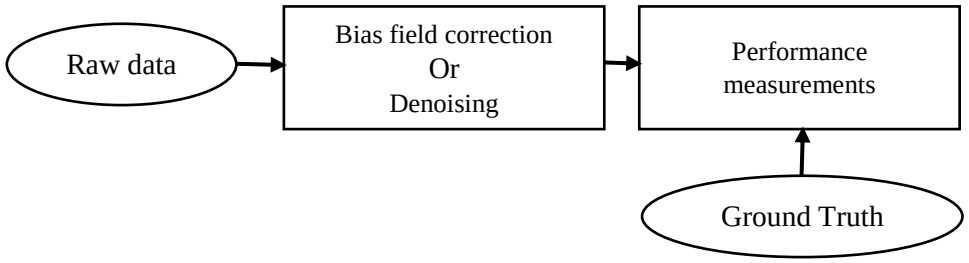

Fig. 1: Generalized block diagram for the Bias field correction or denoising of the images (S. L. # 02~05).

For the last image in the Table 1, both bias field correction and denoising are required which was implemented by the following block diagram.

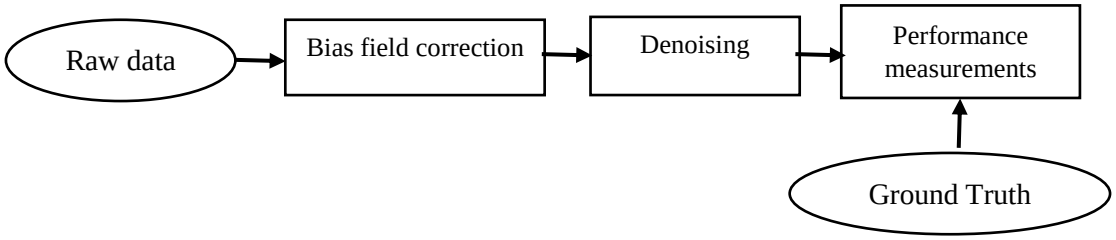

Fig. 2: Generalized block diagram for the Bias field correction and denoising of the images (S. L. #06).

4.1 Results for denoising

For this experiment, some parameters are kept constant trough out the experiments. $Number\ of\ iteration = 25, delta_t = 0.25, kappa = 3, option = 2$. For the isotropic diffusion, there are constant has been fixed as $Constant\ for\ isotropic = 1$ after some of trials and errors. The reason for selecting constant as 1 is shown in Fig.3.

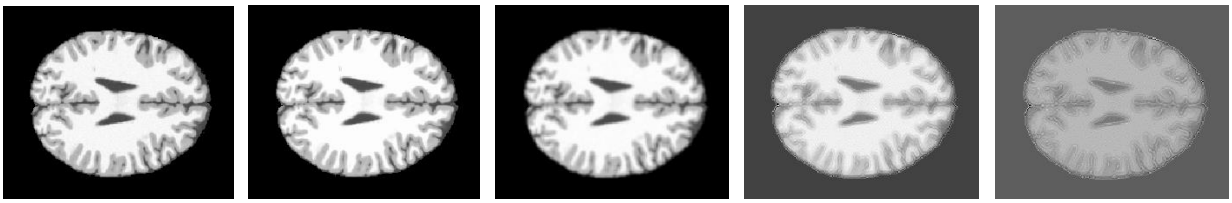

(a) (b) (c) (d) (e)

Fig. 3: Results for isotropic filtering (slice=100) a) original, b) GT, c) constant=1, d) constant=3, and e) constant=5.

From the figure 3, it is seen that when the constant for the isotropic filter increases, the output image becoming more blurred. Hence, suitable value for constant has been select as 1 for the further analysis of the results for denoising.

All the images that required denoising, have been denoised using Anisotropic diffusing, isotropic diffusion and gaussian blurring to compare the effects of each filter. The overall results for all those filtering are shown in Table 2.

Table 2: Quantitative performance for the denoising using Anisotropic, isotropic diffusion and gaussian blurring

Metrics	Images	Anisotropic diffusing	Isotropic diffusion	Gaussian
Entropy Difference	t1_icbm_normal_1mm_pn1_rf0	-0.82179	-0.012383	-0.088112
	t1_icbm_normal_1mm_pn5_rf0	-0.82544	-0.012383	-0.090244
TGD Difference	t1_icbm_normal_1mm_pn1_rf0	1.7061	12.373	36.1354
	t1_icbm_normal_1mm_pn5_rf0	-17.1555	7.2153	35.273
MSE	t1_icbm_normal_1mm_pn1_rf0	15.0686	322.8848	986.3836
	t1_icbm_normal_1mm_pn5_rf0	381.987	425.7638	1000.1735
PSNR	t1_icbm_normal_1mm_pn1_rf0	45.7619	31.9833	27.2094
	t1_icbm_normal_1mm_pn5_rf0	31.7485	30.7806	27.1532
AMBE	t1_icbm_normal_1mm_pn1_rf0	0.020333	0.020333	0.020333
	t1_icbm_normal_1mm_pn5_rf0	0.47275	0.47275	0.47275
CII	t1_icbm_normal_1mm_pn1_rf0	1.0001	1.0001	1.0001
	t1_icbm_normal_1mm_pn5_rf0	1.0033	1.0033	1.0033
SSIM	t1_icbm_normal_1mm_pn1_rf0	0.97505	0.92436	0.8227
	t1_icbm_normal_1mm_pn5_rf0	0.90501	0.89387	0.81821
NCC	t1_icbm_normal_1mm_pn1_rf0	0.99987	0.99564	0.98972
	t1_icbm_normal_1mm_pn5_rf0	0.99678	0.99474	0.98956

In Table 2, it's shown that the first performance parameter Entropy difference in case of Anisotropic diffusion is better than isotropic diffusion and gaussian. It means that the structural information increases more after Anisotropic diffusion than others. So, anisotropic diffusion performs better then rest 2 methods. According to the TGD difference performance evaluation criteria discussed before in section 3.2 the performance of the denoising algorithm is better if the TGD difference is lower. So, in case of anisotropic diffusion, performance is better than other two methods. Algorithm is as better as lower the MSE. From Table 2, Anisotropic has lower MSE than rest methods. On the other hand, the algorithm is better as higher the PSNR, as PSNR is higher as high as low the noise is in the image. In our denoising results, PSNR is higher in anisotropic diffusion. AMBE and CII both are the measure of contrast enhancement. As shown in Table 2, all the three methods perform same, in other words they perform noise removal but have the same amount of effect on the contrast improvement of the original image. SSIM is the measure of the structural preservation. Based on the experimental outcomes, we can say Anisotropic diffusion preserves more

structural information compared to others. NCC measures the similarity between the images, in all cases, we get almost similar outcomes, although Anisotropic diffusion is little better.

For the simplicity of the qualitative measurement here only two slices (slice 70 and slices 115) is shown in Fig. 4. In the case of Gaussian, we can see the processed images is highly blurred compared to Isotropic diffusion which is sharper, but edges are blurred. Compared to Gaussian and Isotropic diffusion, Anisotropic diffused image preserved the most edges and less blurred the processed image which is preferable for the further processing.

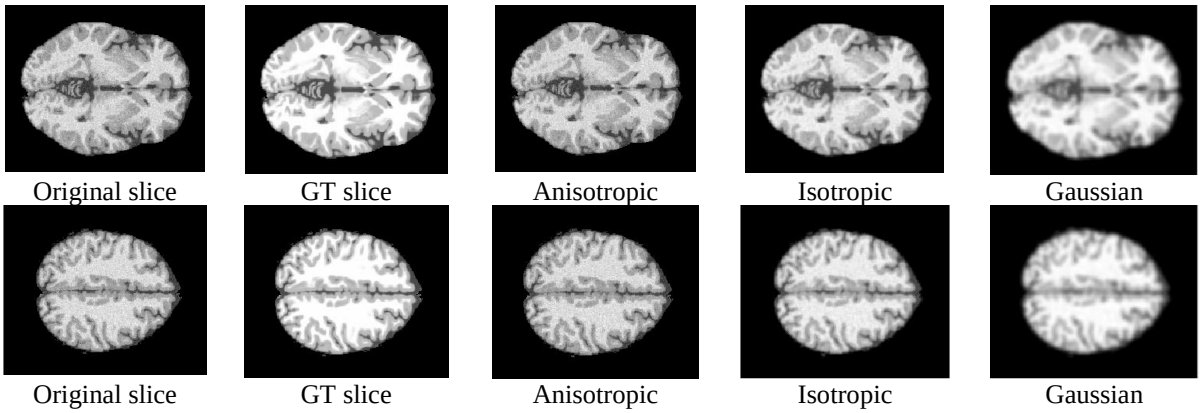

Fig. 4: Qualitative results for denoising where upper row is for slice=70 and lower is for slice=115.

4.2 Results for Bias field correction

This section is dedicated to quantitative and qualitative results for the bias field correction of the given 3D image. Bias field correction can be done using two approaches for example, using 2D implementation in slice by slice or in 3D implementation. For this experiment, some parameters are kept constant trough out the experiments. $Number\ of\ iteration = 20, Number\ of\ region = 3, fuzzifier, q = 1.$

In Table 3, it's shown that the first performance parameter Entropy difference for both 2D and 3D implementation is 0, which means there is no improvement of the entropy after bias field correction. According to the TGD difference performance evaluation criteria discussed before in section 3.2 the performance of the denoising algorithm is better if the TGD difference is lower. So, it can be claim from the Table 3 3D implementation preserve better structural information of the image. In the case of 3D implementation MSE is lower than the 2D implementation which proves less error in 3D implementation. On the other hand, in the 3D implantation the PSNR is high which proves the lower noise also after bias field correction. AMBE and CII both are the measure of contrast enhancement. In case of the 2D implementation the slice by slice processing increase the brightness of the processed image compared to the 3D implementation. SSIM is the measure of the structural preservation. Based on the experimental outcomes, we can say 2D implementation causes less structural deformation compared to 3D implementation. NCC measures the similarity between the images. The experimental outcomes show the better performance of the 2D implementation over 3D implementation.

Table 3: Quantitative performance analysis of the bias field correction (2D and 3D)

Metrics	**Images**	**2D-MICO**	**3D-MICO**
Entropy Difference	t1_icbm_normal_1mm_pn0_rf40	0	0
	t1_icbm_normal_1mm_pn0_rf20	0	0
TGD Difference	t1_icbm_normal_1mm_pn0_rf40	-3.7348	-4.3926
	t1_icbm_normal_1mm_pn0_rf20	-5.3908	-4.3927
MSE	t1_icbm_normal_1mm_pn0_rf40	817.8826	102.6205
	t1_icbm_normal_1mm_pn0_rf20	1291.8235	102.6259
PSNR	t1_icbm_normal_1mm_pn0_rf40	29.4284	34.9941
	t1_icbm_normal_1mm_pn0_rf20	28.0171	34.9939

AMBE	t1_icbm_normal_1mm_pn0_rf40	11.1482	4.3635
	t1_icbm_normal_1mm_pn0_rf20	15.4203	4.3637
CII	t1_icbm_normal_1mm_pn0_rf40	0.98403	0.97671
	t1_icbm_normal_1mm_pn0_rf20	0.99392	0.97672
SSIM	t1_icbm_normal_1mm_pn0_rf40	0.98295	0.93165
	t1_icbm_normal_1mm_pn0_rf20	0.98109	0.93165
NCC	t1_icbm_normal_1mm_pn0_rf40	0.99626	0.94138
	t1_icbm_normal_1mm_pn0_rf20	0.99644	0.94138

Fig. 5 and Fig. 6, shows the bias field corrected images with the corresponding ground truth for the 2D and 3D implementation respectively. From the both Fig. 5 and Fig. 6, is seen that bias field correction for both the implementation either 2D or 3D, work well although their performances are little bit difference as described before. In some context, 2D work well and vice-versa. But, in general 3D implementation works better.

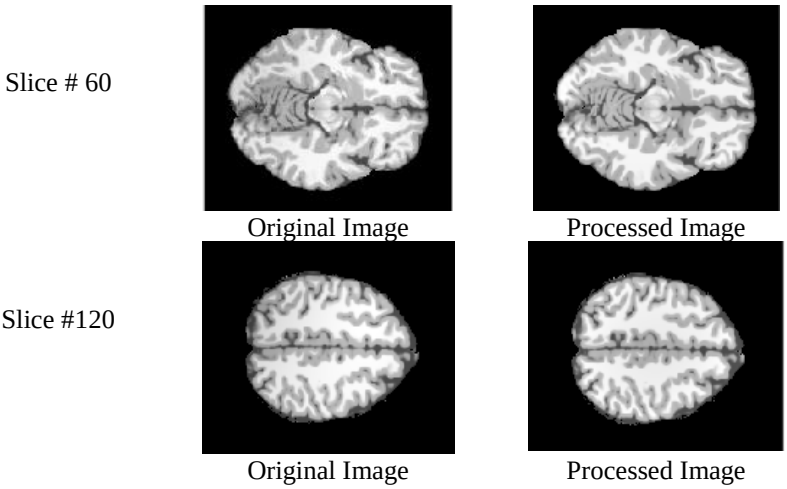

Fig. 5: Qualitative visualization of the bias field correction with 2D implementation

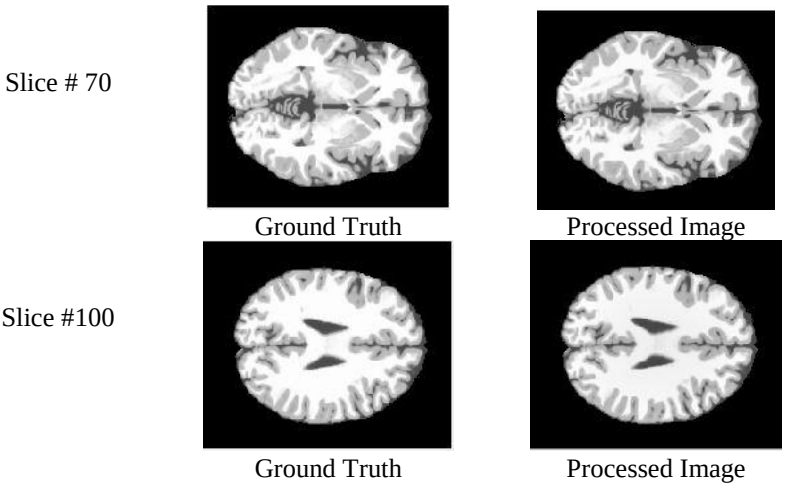

Fig. 6: Qualitative visualization of the bias field correction with 3D implementation

4.3 Results for both Bias field correction and denoising

Table 4 shown the quantitative outcomes of the application of denoising and bias field correction on the SL no. 6 (See Table.1) which has both the noise and bias field. Shown in fig.2 we applied the bias field correction first and then applied the denoising. Compared to previous performance of the algorithms for denoising shown in Table.2, Anisotropic diffusion is used for denoising.

As discussed in the previous sub-section, for the filtering anisotropic diffusion and for bias field correction 3D implementation performed better then others. That why for this image anisotropic diffused and 3D implantation for the bias field correction have been used.

Table 4: Quantitative performance analysis of Denoising and Bias field correction

Metrics	Denoising and Bias field correction
Entropy Difference	0
TGD difference	-21.0016
MSE	524.4315
PSNR	28.0488
AMBE	5.1708
CII	0.9858
SSIM	0.86015
NCC	0.93827

From the table it can be seen that the entropy difference is 0 which means there is no improvement of entropy. TGD difference is negative which indicates TGD is improving. For MSE and PSNR, we can say there is still little bit noise compared to GT. AMBE demonstrate there is contrast enhancement. SSIM shows there is some structural deformation in the processed image. NCC shows the degree of similarity between GT and processed image is quite satisfactory. The qualitative visualization of the processed image along with the GT for the slice no 50 and 100 shown in Fig. 7. Fig.7 qualitatively shows the perfectness of the processed image with the ground truth.

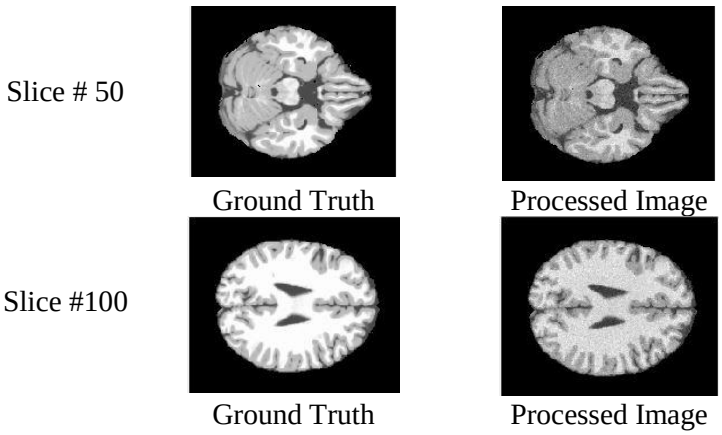

Fig. 7: Qualitative visualization of both bias field correction and denoising

Reference

[1] P. Perona and J. Malik. “Scale-space and edge detection using anisotropic diffusion.” IEEE Transactions on Pattern Analysis and Machine Intelligence, 12(7):629-639, July 1990.

[2] Li, C., Gore, J. and Davatzikos, C. “Multiplicative intrinsic component optimization (MICO) for MRI bias field estimation and tissue segmentation.” *Magnetic Resonance Imaging*, 32(7), pp.913-923, 2014.

[3] Puniani, S. and Arora, S. “*Performance Evaluation of Image Enhancement Techniques*,” International Journal of Signal Processing, Image Processing and Pattern Recognition, 8(8), pp.251-262,2015.

[4] Inflibnetacin. (2018). Inflibnetacin. Retrieved 28 October, 2018, from http://shodhganga.inflibnet.ac.in/bitstream/10603/23580/8/08_chapter 3.pdf

[5] Zhou, W., A. C. Bovik, H. R. Sheikh, and E. P. Simoncelli. "Image Qualifty Assessment: From Error Visibility to Structural Similarity." *IEEE Transactions on Image Processing*. Vol. 13, Issue 4, April 2004, pp. 600–612.